Climate
of the Past

The response of tropical precipitation to Earth's precession: the role of energy fluxes and vertical stability

Chetankumar Jalihal[1,2], Joyce Helena Catharina Bosmans[3,a,b], Jayaraman Srinivasan[2], and Arindam Chakraborty[1,2]

[1]Centre for Atmospheric and Oceanic Sciences, Indian Institute of Science, Bangalore, India
[2]Divecha Centre for Climate Change, Indian Institute of Science, Bangalore, India
[3]Department of Environmental Science, Radboud University, Nijmegen, the Netherlands
[a]formerly at: Faculty of Geosciences, Utrecht University, Utrecht, the Netherlands
[b]formerly at: Royal Netherlands Meteorological Institute (KNMI), De Bilt, the Netherlands

Correspondence: Chetankumar Jalihal (jalihal@iisc.ac.in)

Abstract. The changes in Earth's precession have an impact on the tropical precipitation. This has been attributed to the changes in seasonal solar radiation at the top of the atmosphere. The primary mechanism that has been proposed is the change in thermal gradient between the two hemispheres. This may be adequate to understand the zonal mean changes, but cannot explain the variations between land and oceans. We have used a simple model of the intertropical convergence zone (ITCZ) to unravel how precipitation changes with precession. Our model attributes the changes in precipitation to the changes in energy fluxes and vertical stability. We include the horizontal advection terms in this model, which were neglected in the earlier studies. The final response of the land and oceans is a result of complex feedbacks triggered by the initial changes in the insolation. We find that the changes in precipitation over the land are mainly driven by changes in insolation, but over the oceans, precipitation changes on account of changes in surface fluxes and vertical stability. Hence insolation can be a trigger for changes in precipitation on orbital timescales, but surface energy and vertical stability play an important role too. The African monsoon intensifies during a precession minimum (higher summer insolation). This intensification is mainly due to the changes in vertical stability. The precipitation over the Bay of Bengal decreases for minimum precession. This is on account of a remote response to the enhanced convective heating to the west of the Bay of Bengal. This weakens the surface winds and thus leads to a decrease in the surface latent heat fluxes and hence the precipitation.

1   Introduction

The most dominant temporal mode in insolation and tropical precipitation is the 23 000-year precession cycle of the Earth (Berger, 1978; Kutzbach, 1981; Pokras and Mix, 1987). Both proxy (Wang et al., 2007; Wang et al., 2008; Cruz Jr. et al., 2005) and model (Kutzbach, 1981; Kutzbach et al., 2008; Tuenter et al., 2005; Weber and Tuenter, 2011; Caley et al., 2014; Shi, 2016) based studies suggest that the intensities of monsoons have varied in proportion to insolation on orbital timescales. When changes in precession increase the insolation in the Northern Hemisphere, the zonal mean precipitation band shifts northward on account of the increase in thermal gradient between the two hemispheres (Donohoe et al., 2013; Schneider et al., 2014; Kang et al., 2008). This mechanism cannot explain the longitudinal changes in precipitation (Mohtadi et al., 2016). The simulation of climate models shows that precipitation over land and oceans responds differently to precessional forcing (Clement et al., 2004; Tuenter et al., 2003; Chamales, 2014). This has been observed in the idealized as well as realistic precession experiments with climate models (e.g., Braconnot et al., 2008; Zhao and Harrison, 2012; Bosmans et al., 2015).

It is attributed to the land–sea contrast theory in the previous studies (Zhao and Harrison, 2012; Bosmans et al., 2012). The land warms more than the surrounding ocean due to its lower thermal inertia. Hence a low pressure develops over land and a monsoon circulation is established. The increase in insolation leads to deeper thermal lows over land, which enhance the onshore flow of moisture-laden winds. This leads to stronger ascent over land and an increase in precipitation. This thermal contrast, however, disappears after the onset of monsoon due to the cooling of land by precipitation and cloud cover. In fact, in good monsoon years, the land surface temperature is lower (Gadgil, 2018).

Some studies have used the changes in energy balance to understand the response of precipitation to precession (Braconnot et al., 2008; Hsu et al., 2010; Merlis et al., 2013; Chamales, 2014; Battisti et al., 2014). Braconnot et al. (2008) suggested that the net energy in the atmosphere over land and adjacent oceans changes due to precession. The atmosphere then acts to redistribute the excess energy, thereby setting up a land–ocean difference in precipitation. Hsu et al. (2010) showed that the precipitation changes due to precession are related to the changes in the total column energy, which drives changes in vertical velocity. Chamales (2014) on the other hand has argued that the stability over oceans changes, whereas land regions respond by transporting the excess moist static energy. These are, however, generalizations for the entire tropics. The role of local processes and feedbacks might be important in driving regional changes in precipitation. Thus, individual regions need to be studied separately to understand the cause of the changes. For example, Battisti et al. (2014) suggested that higher summer insolation leads to a migration of the near-surface moist static energy from the Bay of Bengal to India, before the onset of monsoon. They argued that hence the precipitation centroid shifts to India.

Moisture and MSE equations can be used separately to understand the dynamics of monsoon under different climate scenarios (Sun et al., 2016, 2018). In this work, we follow Neelin and Held (1987) and demonstrate the advantage of combining the two equations. The resulting simple model attributes precipitation to energy fluxes and vertical stability of the atmosphere. This model, however, can only be used for regions where moisture and temperature gradients are weak. In this paper, we propose a modified version of the simple model which takes into account the horizontal gradients as well. We have used time-slice experiments in a high-resolution general circulation model (GCM), EC-Earth (Bosmans et al., 2015). This GCM was run in two orbital configurations which correspond to the extremes in precession (Fig. 1). The advantage of doing this is that the amplitude of the response is large, while the spatial pattern is similar to a simulation of realistic precession such as the Mid-Holocene (MH).

The paper is organized as follows. The next section describes the model and the experimental setup, and outlines the derivation of a simple model for the intertropical conver-

gence zone (ITCZ). We have used this simple ITCZ model to understand the factors leading to the shift in precipitation between land and oceans, at the regional scale. The results are described in Sect. 3. It is followed by a discussion about the precipitation response to MH and obliquity forcing with the help of the simple ITCZ model.

## 2 Experimental design and analysis method

2.1 Climate model description

EC-Earth is a fully coupled ocean–atmosphere GCM (Hazeleger et al., 2010, 2012). We have used model version 2.2. The Integrated Forecasting System (IFS) was the atmospheric component. The spectral resolution was T159 (roughly $1.125° \times 1.125°$) with 62 vertical levels. The convective scheme (Bechtold et al., 2008) was used along with the Balsamo et al. (2009) H-TESSEL land surface scheme, including surface runoff. The Nucleus for European Modeling of the Ocean (NEMO, version 2) was the ocean component. The horizontal resolution was 1° with 42 vertical levels (Madec, 2008; Sterl et al., 2012). NEMO includes sea-ice model LIM2. The OASIS3 coupler (Valcke and Morel, 2006) couples the ocean, sea ice, land, and atmosphere. EC-Earth performs well for the present day when compared to CMIP3 models in terms of climatology as well as inter-annual, spatial, and temporal variability (Hazeleger et al., 2010, 2012).

2.2 Experimental designs

The two precession extremes, precession minima P_{min} and precession maxima P_{max}, correspond to summer solstice at perihelion and winter solstice at perihelion, respectively (Fig. 1). Table 1 shows the orbital configurations used. This leads to a stronger seasonal cycle in the Northern Hemisphere (NH) and a weaker seasonal cycle in the Southern Hemisphere (SH) in P_{min} (Fig. 2). On the other hand, the seasonal cycle is weaker in the NH and stronger in the SH in P_{max}.

The model is run separately for each of the orbital configurations. The length of each simulation is 100 years, with the first 50 years being considered spinup. We have used the climatology of the last 50 years, for all our analysis. The orbital parameters remain constant throughout the simulation. All other boundary conditions (e.g., the solar constant, greenhouse gas concentrations, orography, ice sheets, vegetation) were kept constant at the pre-industrial levels. Vernal equinox has been fixed at 21 March, and the present-day calendar is used. Since the length of the season and the dates of equinoxes change along the precession cycle, the autumn equinoxes do not coincide. This is known as the "calendar effect". It introduces some errors due to the phasing of insolation. We do not make any corrections in order to be consistent with previous studies. Further details about the experiments are provided in Bosmans et al. (2015).
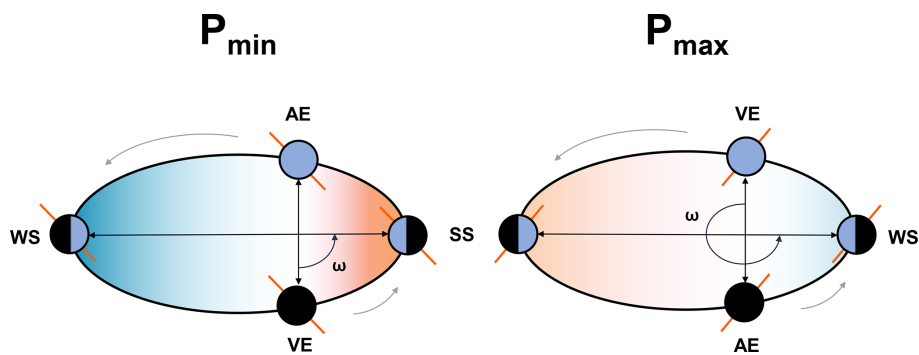
Figure 1. The schematic diagram showing the orbital configuration of minimum precession (P_{min}) and maximum precession (P_{max}). In P_{min}, summer solstice (SS) occurs at perihelion, while in P_{max}, winter solstice (WS) coincides with the perihelion. AE and VE are the autumn and vernal equinoxes, respectively.

Table 1. The orbital configuration used for the extremes in precession, precession minima P_{min}, precession maxima P_{max}, and the pre-industrial. "e" represents eccentricity, δ is the tilt, and ω is the longitude of perihelion. The values of these have been chosen based on the extremes in the precession parameter $e * \sin(\pi + \omega)$ that have occurred in the last 1 Myr (Berger, 1978). Pre-industrial values are shown for comparison.

	Eccentricity, e	Obliquity, δ (°)	Longitude of perihelion, ω (°)
Pre-industrial	0.017	23.45	282.04
P_{min}	0.056	22.08	95.96
P_{max}	0.058	22.08	273.5

Table 2. The regions used in this article and their coordinates.

Region	Co-ordinates
Northern tropics	(0–30° N; 0–360° E)
Southern tropics	(30° S–0° N; 0–360° E)
Central India	(15–25° N; 73–83° E)
Bay of Bengal	(10–20° N; 85–95° E)
Southeast Asia	(0–25° N; 100–125° E)
Arabian Sea	(10–20° N; 60–70° E)
Northern Africa	(5–15° N; 20° W–0° E)
Brazil	(20–10° S; 70–50° W)
South Atlantic	(20–10° S; 30° W–0° E)
South Africa	(20–10° S; 15–35° E)
Northern Australia	(25–15° S; 130–140° E)

2.3 Diagnostic methodology

The Hadley cell is a thermally direct overturning circulation in the tropics. It takes energy away from the tropics and transports it towards the poles. The Hadley cell has a rising branch in the deep tropics and a descending branch in the extratropics. This leads to moisture convergence near the rising branch. The ITCZ coincides with the rising branch of the Hadley cell and is responsible for the zone of heaviest precipitation in the tropics. The characteristics of the ITCZ can be described by using the conservation equations for moist static energy (MSE) and moisture. Using this approach, Neelin and

Held (1987) proposed a simple model for ITCZ in terms of net energy input into the atmosphere and vertical stability. This is a diagnostic model that has been used to explain variations in rainfall due to global warming (Chou and Neelin, 2004; Chou et al., 2006) and the impacts of aerosols (Chou et al., 2005). In this section, we have discussed this simple model in detail. Equations (1) and (2) correspond to the conservation of MSE and moisture in a vertical column of the atmosphere. The first term in both the equations is horizontal divergence, with the second term being the vertical divergence of MSE and moisture fluxes, respectively.

The quantities on the right-hand side are the sum of all sources and sinks. Further details on the derivation of Eq. (1) can be found in Neelin and Held (1987). The time derivatives have been dropped in these equations because the climate is assumed to be in a steady state. The angle brackets ($\langle \rangle$) indicate vertical integral.

$$\langle \nabla \cdot m\mathbf{U} \rangle + \left\langle \frac{\partial m\omega}{\partial p} \right\rangle = Q_{\text{div}}, \tag{1}$$
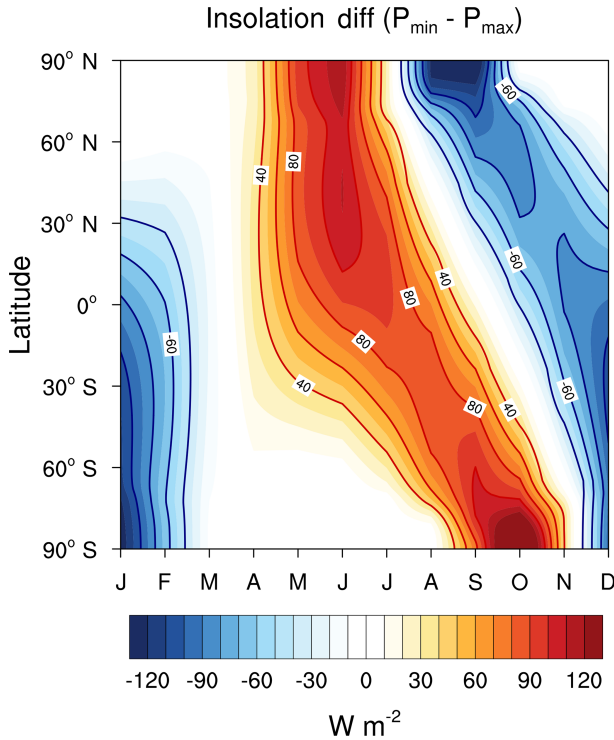
$$\langle \nabla \cdot q\mathbf{U} \rangle + \left\langle \frac{\partial q\omega}{\partial p} \right\rangle = E - P, \tag{2}$$

$$\langle A \rangle = -\int_{P_b}^{P_t} A \frac{dp}{g}, \tag{3}$$

where P is the precipitation rate (mm day^{-1}). E is the evaporation rate (mm day^{-1}). Q_{div} is the total column energy,

Insolation diff (P_min - P_max)

Figure 2. The difference in the incoming solar radiation at the top of atmosphere between P_{min} and P_{max} as a function of latitude and month.

i.e., the sum of all the energy fluxes into the atmosphere (Eq. 4) (in mm day^{-1}; taking the latent heat of vaporization as 2.26×10^6 J kg^{-1}, we get 1 mm day$^{-1} = 26.16$ W m^{-2}). Over land since the storage term is small, the sum of all the energy fluxes at the surface is small. Hence, Q_{div} is mainly governed by the fluxes at the top of atmosphere (TOA). However, over oceans the contribution of surface fluxes is large. q is specific humidity (kg kg^{-1}). m is moist static energy (J kg^{-1}), which is the sum of internal energy, potential energy, and moist energy ($C_p T + gZ + L_v q$). P_b is the pressure at the bottom of the atmospheric column (Pa). P_t is the pressure at the top of the atmospheric column (Pa). g is the acceleration due to gravity (m s^{-2}). The full equation for Q_{div} is

$$Q_{div} = \underbrace{LHF + SHF + Net\_Sfc\_Rad}_{\text{bottom fluxes}}$$
$$+ \underbrace{Net\_TOA\_LW + Net\_TOA\_SW}_{\text{TOA Fluxes}}. \tag{4}$$

where LHF is surface latent heat flux (mm day^{-1}). SHF is surface sensible heat flux (mm day^{-1}). Net_Sfc_Rad is net surface radiation (long wave + short wave) (mm day^{-1}). Net_TOA_LW is net top of atmosphere longwave radiation (mm day^{-1}). Net_TOA_SW is net top of atmosphere short-wave radiation (mm day^{-1}). Clubbing all the radiation fluxes

together into one quantity "Q_{rad}", we get

$$Q_{div} = LHF + SHF + Q_{rad}. \tag{5}$$

Assuming $\omega = 0$ at the top as well as the surface leaves us with the horizontal terms only. The governing equations can be combined and simplified as

$$P - E = \frac{Q_{div}}{GMS}, \tag{6}$$

$$GMS = \frac{m_1 - m_2}{L_v(q_2 - q_1)}, \tag{7}$$

$$m_1 = \frac{\int_{P_t}^{P_m} m \nabla \cdot \boldsymbol{U} dp/g}{\int_{P_t}^{P_m} \nabla \cdot \boldsymbol{U} dp/g}, \tag{8}$$

$$m_2 = \frac{\int_{P_m}^{P_b} m \nabla \cdot \boldsymbol{U} dp/g}{\int_{P_m}^{P_b} \nabla \cdot \boldsymbol{U} dp/g}, \tag{9}$$

where GMS is the gross moist stability, as obtained by taking the ratio of Eqs. (2.11) and (2.12) from Neelin and Held (1987). m_1 and m_2 are, respectively, the total MSE in the upper (mid troposphere to top) and lower troposphere (surface to mid troposphere), normalized by the divergence of that layer. Thus, GMS is mainly a function of vertical profiles of MSE, and it provides a measure of vertical stratification of the atmosphere. P_m is pressure at the mid-troposphere level. Similarly, q_1 and q_2 represent the total moisture in the upper and lower troposphere, normalized by divergence. The mass convergence in the lower troposphere is the same as the mass divergence in the upper troposphere. The horizontal variations of temperature and moisture are assumed to be weak within the tropics. This implies that the horizontal advection of temperature and moisture is small. This simple model attributes the changes in $P - E$ to either the changes in total column energy or the vertical stability.

Figure 3a shows a scatter of $P - E$ as a function of Q_{div} for the 3 summer months June, July, and August taken separately. The scatter is made for central India, the Bay of Bengal, and northern Africa for each of the precession extremes. We chose these three regions to highlight that neglecting the role of horizontal advection may not always be appropriate. The plot shows that the two are nearly linear, as indicated by the simple model (Eq. 6). The slight deviations from linearity are due to variations in GMS. As we go from P_{max} to P_{min} (low to high insolation in NH summer), both Q_{div} and $P - E$ increase over central India and northern Africa (land regions). However, both these quantities decrease over the Bay of Bengal (oceanic region). The net energy input into the atmosphere and thus Q_{div} is positive for all these regions during the summer.

We have shown in Fig. 3b a scatter of $P - E$ vs. GMS for the same regions. The figure shows that there is no definite relation between the two. Equation (6) suggests that all values for GMS should be positive since $P - E$ and Q_{div} are
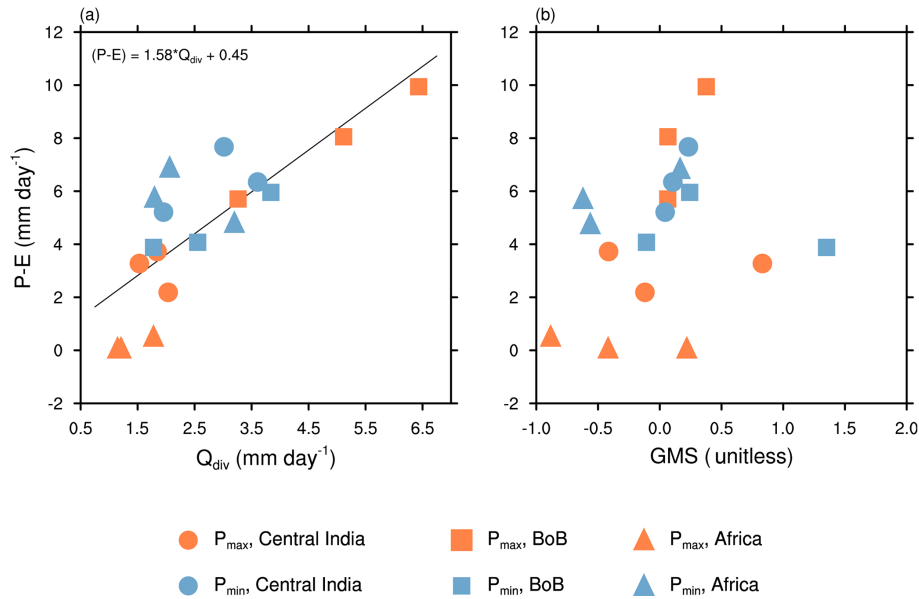
Figure 3. The dependence of $P - E$ on **(a)** Q_{div} and **(b)** GMS, for three regions: central India (15–25° N; 73–83° E), the Bay of Bengal (10–20° N; 85–95° E), and Africa (5–15° N; 20° W–0° E). The months Jun–Jul–Aug are taken separately. The blue and orange symbols correspond to P_{min} and P_{max}, respectively.

both positive. There are, however, some points in the scatter where GMS is negative. This indicates that the assumption about the horizontal advection being small is not always valid. Hence, we modify the definition of GMS to include the horizontal advection terms.

By taking the ratio of Eqs. (1) and (2), after multiplying Eq. (2) by L_v (the latent heat of vaporization for water), we get

$$P - E = \frac{Q_{div}}{\text{TGMS}}, \tag{10}$$

$$\text{TGMS} = \frac{\left\langle \nabla \cdot m\boldsymbol{U} + \frac{\partial m\omega}{\partial p} \right\rangle}{-L_v \left\langle \nabla \cdot q\boldsymbol{U} + \frac{\partial q\omega}{\partial p} \right\rangle}, \tag{11}$$

where TGMS stands for total GMS (the term "total" indicates inclusion of all advection terms). TGMS is based on only one assumption, that the time derivatives of m and q are negligible. This is a good assumption for seasonal mean conditions. TGMS is particularly useful for smaller regions, where horizontal advection can be large. TGMS represents how efficiently an atmospheric column can diverge MSE per unit moisture converged into the column. TGMS is an extension of the concept of GMS, with horizontal advection terms included. This suggests that, along with the energy fluxes and vertical stratification of a column, the lateral transport of MSE and moisture determine the precipitation. A value of TGMS similar in magnitude to GMS indicates that the horizontal transport of MSE is negligible. A change in TGMS between two climates would suggest that the transport of MSE has changed. We have used the equivalence in Eqs. (1) and

(2) to estimate TGMS. Since our goal is not to estimate the changes in $P - E$ but to diagnose the cause of these changes, there is no need to make an independent estimate of TGMS.

To quantify the relative contribution of Q_{div} and TGMS to the changes in $P - E$, we do the following. Writing Eq. (10) for P_{max},

$$P - E = \frac{Q}{G}, \tag{12}$$

where P, E, Q, and G are precipitation, evaporation, Q_{div}, and TGMS, respectively. Considering P_{max} as the reference case and P_{min} as the perturbed case, we can write the following for P_{min}:

$$(P + \Delta P) - (E + \Delta E) = \frac{Q + \Delta Q}{G + \Delta G}, \tag{13}$$

where Δ represents the perturbation from P_{max}. Now dividing by $P - E$, we get

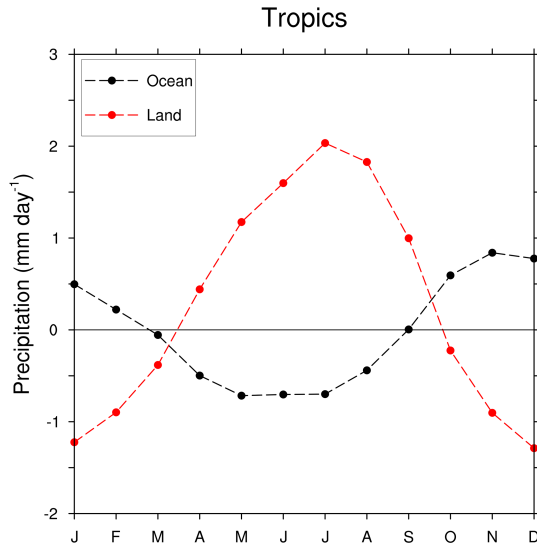$$1 + \frac{\Delta(P - E)}{(P - E)} = \frac{1 + \Delta Q/Q}{1 + \Delta G/G}. \tag{14}$$

This equation can further be modified as

$$\underbrace{\Delta(P - E)}_{\text{Change in } P - E} = \underbrace{\frac{\frac{\Delta Q}{Q}}{1 + \frac{\Delta G}{G}}(P - E)}_{\text{Contribution from } Q_{div}} + \underbrace{\frac{-\frac{\Delta G}{G}}{1 + \frac{\Delta G}{G}}(P - E)}_{\text{Contribution from TGMS}}. \tag{15}$$

3 Results

In this section, we have explained the changes in $P - E$ between P_{min} and P_{max} in terms of Q_{div} and TGMS. We start

Figure 4. The difference in precipitation ($P_{min} - P_{max}$) for all the tropical land and ocean taken separately (30° S–30° N).

by giving an overview of the entire tropics and then we look at the South Asian monsoon in detail.

3.1 Response of tropical precipitation to precession

3.1.1 Spatial patterns of the response

Figure 4 shows the difference in precipitation between P_{min} and P_{max} averaged over the tropical land and oceans separately. Precipitation change over the tropical land is out of phase with the changes in precipitation over the oceans. The amplitude of the change is higher over land than over oceans. Furthermore, over land, the change is of a higher magnitude during the boreal summer than the austral summer. This implies that the Northern Hemisphere monsoons are more sensitive to precession than the Southern Hemisphere monsoons. The vernal equinoxes during P_{min} and P_{max} occur on 21 March. Therefore, the difference in insolation between the two cases is very small during March. Hence the changes in land and ocean precipitation have a zero crossing during this month. Since we are interested in regions where there is moisture convergence, our analysis will focus on $P - E$ instead of precipitation.

In Fig. 5, the spatial patterns of the changes in $P - E$ and Q_{div} are shown averaged over JJA (panels (a) and (b)) and DJF (panels (c) and (d)). First, we discuss the changes in precipitation during JJA. Most of the land regions in the Northern Hemisphere show an increase in $P - E$. The African monsoon has strengthened substantially in P_{min}, with an increase of about $10 \, \text{mm} \, \text{day}^{-1}$. $P - E$ has, in general, decreased over the oceans. However, there are many regions over the oceans (e.g., the Arabian Sea) where $P - E$ has increased. Hence, the amplitude of the changes in $P - E$ is small when averaged over all the tropical oceans (Fig. 4). The

changes in Q_{div} have a pattern similar to that of $P - E$, with positive values over most of the land regions, and both positive and negative values over the oceanic regions. This is due to the direct relation between $P - E$ and Q_{div} as suggested by the simple model. There are, however, some exceptions like the Arabian Sea and Africa. Q_{div} has decreased over the Arabian Sea, but $P - E$ has increased. The regions of the largest increase in $P - E$ and Q_{div} are not co-located over Africa. These are on account of the changes in TGMS.

During DJF, P_{min} has less insolation (Fig. 2), and correspondingly a decrease in $P - E$ and Q_{div} is seen over the land regions (Fig. 5c and d). Over oceans, there are regions of both positive and negative changes in $P - E$ during DJF as well. The magnitude of changes in Q_{div} is on a similar order during JJA and DJF. However, the changes in $P - E$ are larger during JJA compared to DJF.

3.1.2 Dominant factors determining the response of tropics

In this section, we look at the various terms in Eq. (15) for different regions of the tropics (Fig. 6). Panels (a) and (b) are for the Northern Hemisphere and Southern Hemisphere, respectively. The analysis was done for the summer months of the respective hemispheres (JJA for the Northern Hemisphere and DJF for the Southern Hemisphere). The blue bar represents the changes in $P - E$, whereas the light red and dark red bars are contributions from Q_{div} and TGMS. Q_{div} explains most of the changes in $P - E$ when all the land regions in the northern tropics are taken together. This need not be true in smaller regions. For example, TGMS contributes most to the changes in $P - E$ over Africa. Because $P - E$ has a different sign over various oceanic regions, the change in $P - E$, averaged over all the tropical oceans, is small. The contributions from Q_{div} and TGMS are in opposite directions, thus almost canceling each other out. The contribution from TGMS is, however, slightly higher. The Arabian Sea shows an increase in $P - E$, due to a change in TGMS. The decrease in $P - E$ over the Bay of Bengal is, however, mainly due to changes in Q_{div}, with the changes in TGMS being small.

In the southern tropics the dominant contribution is from changes in Q_{div} over land and changes in TGMS over oceans. In the cases of South Africa and Brazil changes in TGMS and Q_{div} make an equal contribution. TGMS drives most of the changes in $P - E$ over northern Australia and the South Atlantic. Figure 6 highlights the fact that the mechanisms for the changes in precipitation are region specific. Hence, each region must be studied separately to understand the physical mechanism that caused the changes in $P - E$. Both the Indian land mass and the Bay of Bengal are part of the Indian monsoon system, yet they demonstrate a different response to the precessional forcing. Hence, we discuss this asymmetric response in detail in the following subsection. Such an asymmetry also exists within the East Asian monsoon, which has been discussed in a separate subsection.
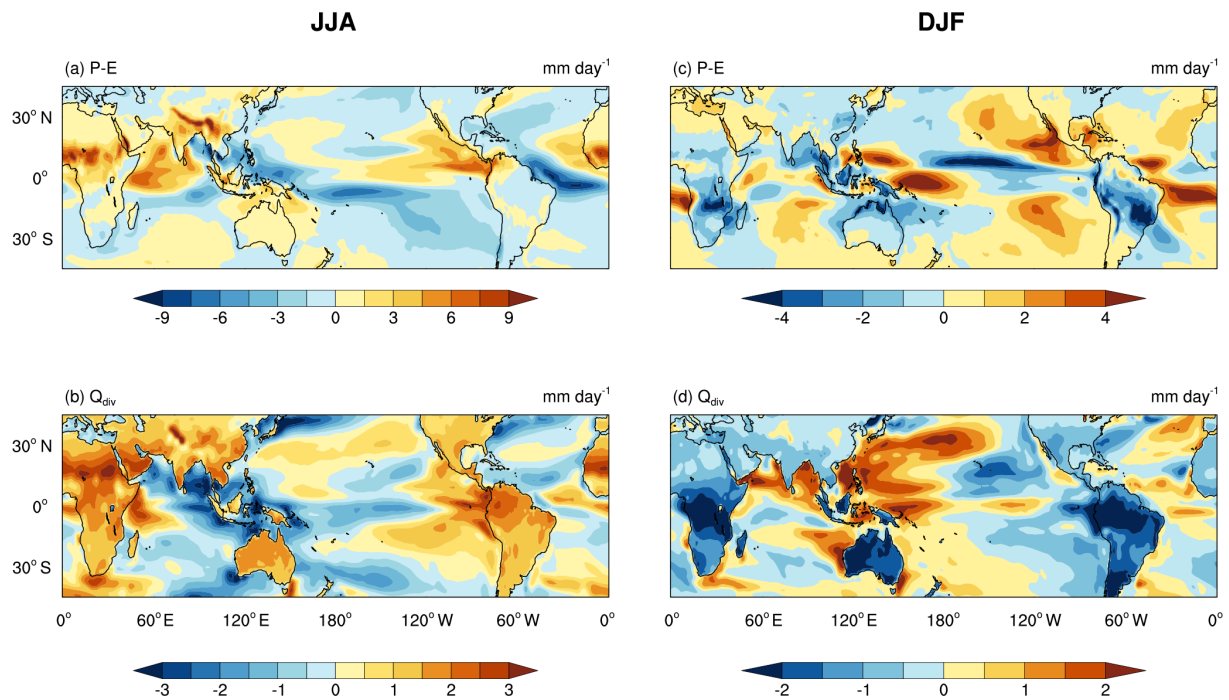
Figure 5. The difference in $P - E$ **(a, c)** and Q_{div} **(b, d)**. **(a)** and **(b)** are for the JJA mean and **(c)** and **(d)** are for the DJF mean.
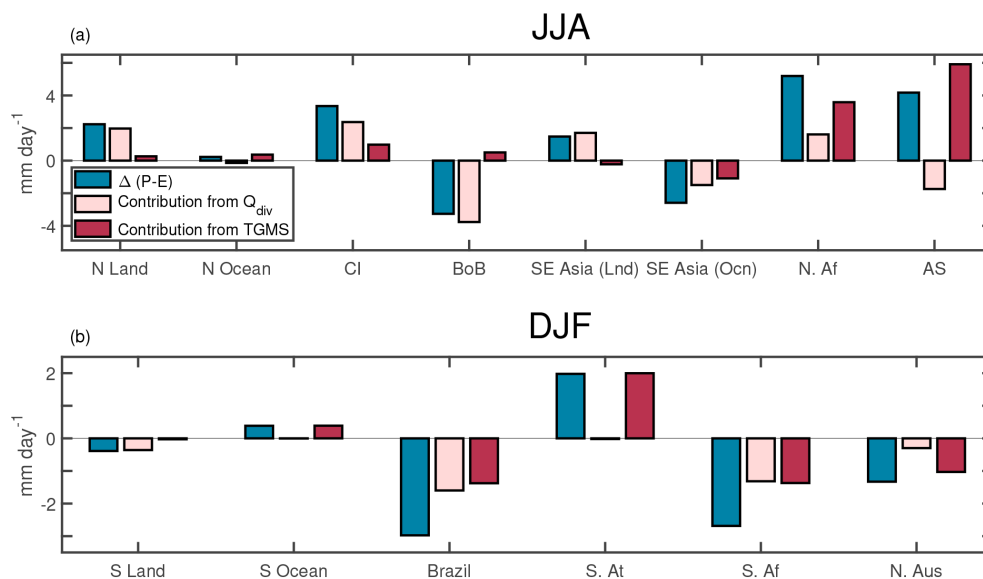
Figure 6. The contribution of Q_{div} and TGMS to the changes in $P - E$. **(a)** is for the JJA mean and regions in the Northern Hemisphere, while **(b)** is for regions in the Southern Hemisphere and averaged over DJF. The blue bar is the change in $P - E$, while pink and red bars represent the contribution from Q_{div} and TGMS. The abbreviations used in **(a)** are *N Land*: northern tropics (land only), *N Ocean*: northern tropics (ocean only), *CI*: central India, *BoB*: the Bay of Bengal, *SE Asia (Lnd)*: Southeast Asia (land only), *SE Asia (Ocn)*: Southeast Asia (ocean only), *N. Af*: northern Africa, and *AS*: Arabian Sea, and in **(b)**, *S Land*: southern tropics (land only), *S Ocean*: southern tropics (ocean only), *S. At*: South Atlantic, *S. Af*: South Africa, and *N. Aus*: northern Australia. The coordinates of these regions are provided in Table 2.
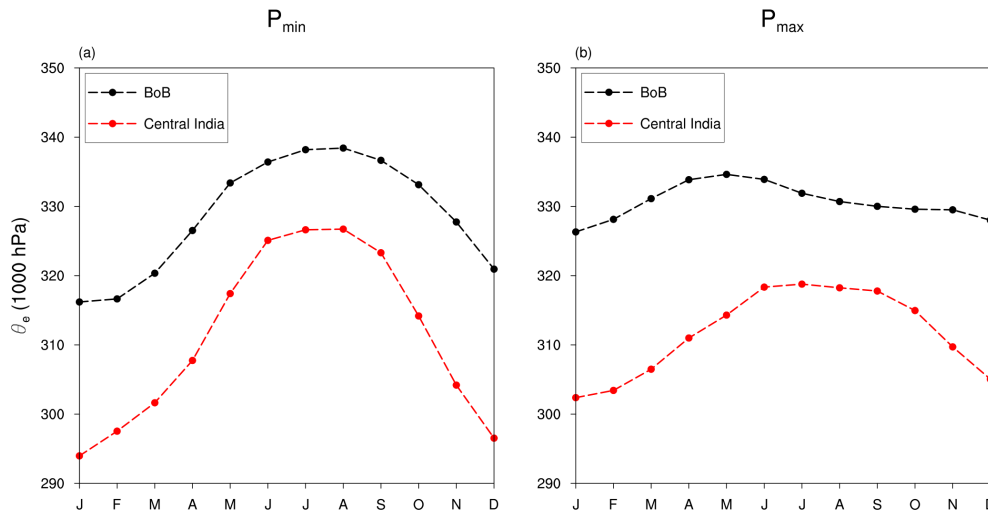
Figure 7. The seasonal cycle of near-surface equivalent potential temperature (θ_e) for India and the Bay of Bengal for the **(a)** P_{min} configuration and **(b)** P_{max}.

3.2 Explaining the response of the Indian monsoon to precession

Battisti et al. (2014) suggested that different response of the Indian land mass and the Bay of Bengal is due to migration of near-surface equivalent potential temperature from the Bay of Bengal over to India. This is because the rate of increase in insolation is higher in the high insolation (similar to P_{min}) experiment. This causes the equivalent potential temperature θ_e to rise rapidly over India. It is known that the location of ITCZ coincides with that of the surface energy maxima (Privé and Plumb, 2007a, b; Bordoni and Schneider, 2008; Boos and Kuang, 2010). Hence ITCZ migrates over India quickly and remains there. However, EC-Earth simulates higher near-surface equivalent potential temperature θ_e over the Bay of Bengal, in both P_{min} and P_{max} (Fig. 7). In this section, we propose an alternate mechanism for the different response of the Indian land mass and the Bay of Bengal to the changes in precession.

We have shown earlier that in P_{min} there is an increase in Q_{div} over the Indian land mass and a decrease over the Bay of Bengal with respect to P_{max} (Figs. 3 and 6). Here we examine the factors that caused the changes in Q_{div}. Splitting Q_{div} into its component fluxes (Eq. 5) will help us to determine which flux contributed the most. Figure 8 is a spatial map of the differences in $P - E$, Q_{div} and its component fluxes Q_{rad}, LHF, and SHF. Q_{div} has a good spatial coherence with $P - E$, over most of the regions except the Arabian Sea. As was discussed earlier, this is due to the changes in TGMS, which is able to counter the effect of reduced Q_{div}. $P - E$ has decreased along the southern parts of the Western Ghats but has increased in the northern parts of the Western Ghats. Q_{rad} bears a resemblance to $P - E$. This suggests that radiative feedbacks from clouds are present. Changes in Q_{rad} are not large enough to counter the decrease in latent heat flux

(LHF) over the Arabian Sea and the Bay of Bengal. Thus, the decrease in LHF over these regions reduces Q_{div} there. In fact, Q_{div} and LHF have similar spatial patterns over the oceanic regions. The changes in sensible heat flux (SHF) are small in most places.

We take two regions: one over central India and the other over the Bay of Bengal, to identify the flux which contributes most to the changes in Q_{div}. These regions are outlined with black boxes in Fig. 8a. The changes in the three components of Q_{div} over these two regions are depicted in the bar chart (Fig. 8f). It shows the dominance of the radiative terms over India, and LHF over the Bay of Bengal, respectively.

LHF is a function of surface wind speed, sea surface temperature (SST), and near-surface relative humidity. LHF increases with an increase in SST and wind speed. SST has increased over the Bay of Bengal and southern Arabian Sea by about 2 °C (Supplement Fig. S1). Thus, it cannot explain the decrease in LHF. Hence, we look at the changes in wind speed (Fig. 9). Fig. 9a and b show the mean winds at 850 hPa. The shading indicates wind speed and the streamlines show the direction of flow. The axis of the low-level jet (LLJ) has shifted to the north, and this has led to a decrease in winds over the Bay of Bengal. Due to LLJ, deep oceanic water upwells along the coast of Somalia. This leads to cooler SSTs over the western parts of the Arabian Sea. Since in P_{min}, LLJ has shifted further north, the region of upwelling also shifts north, thus leading to cooler SSTs in the western coast of the northern Arabian Sea (Fig. S1). Hence, LHF over the Arabian Sea decreases due to weaker winds in the southern parts and colder SST in the northern parts.

The shift in LLJ leads to lesser moisture flux along the southern part of the Western Ghats. Hence, $P - E$ decreases there. At the same time, the LLJ brings more moisture into the northern parts of the Western Ghats, leading to increase
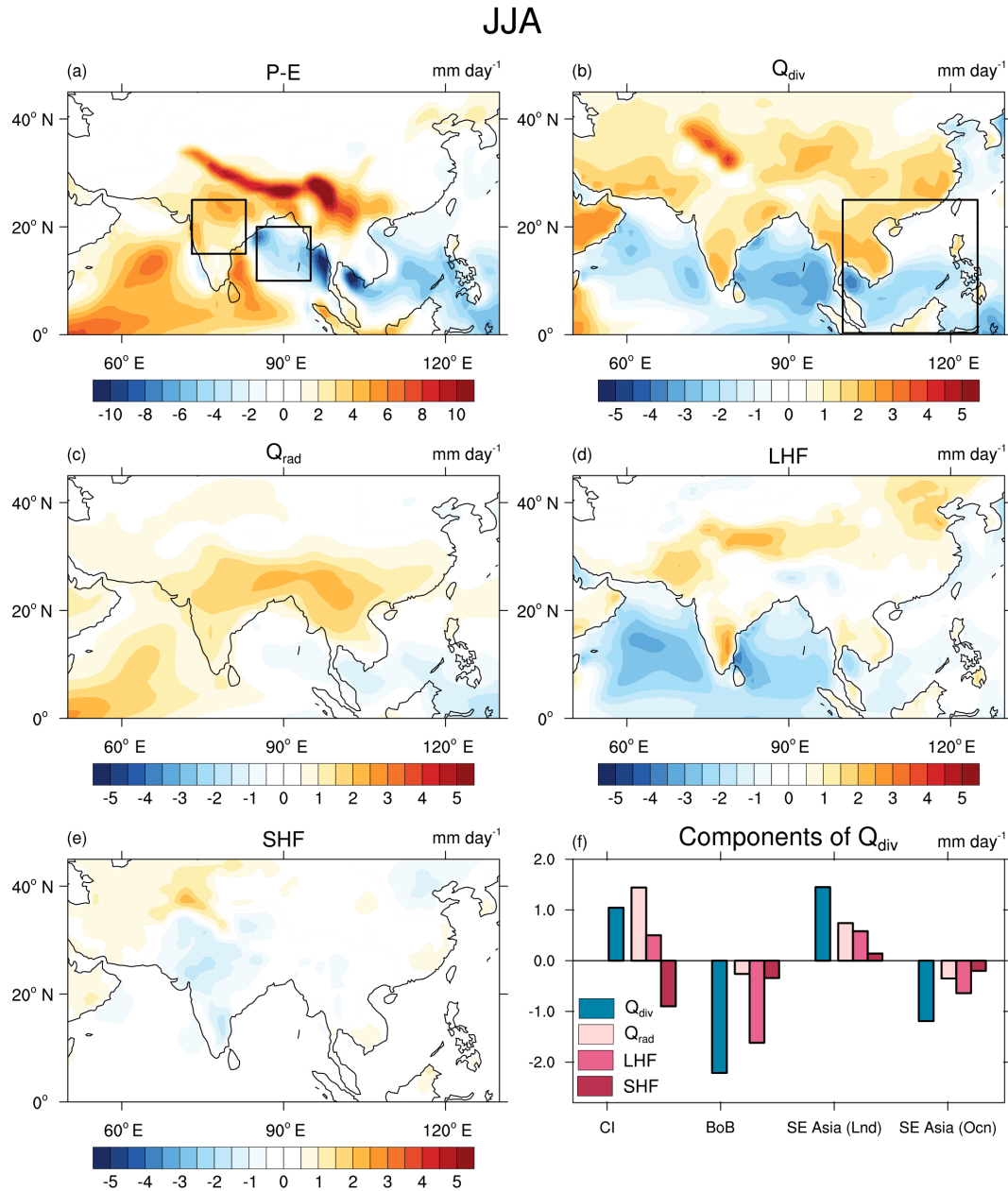
Figure 8. The JJA mean difference ($P_{\mathrm{min}} - P_{\mathrm{max}}$) in (**a**) $P - E$, (**b**) Q_{div} (sum of energy fluxes at the top and bottom of the atmosphere), (**c**) Q_{rad} (sum of all radiative fluxes at the top and bottom of the atmosphere), (**d**) latent heat flux, and (**e**) sensible heat flux. The boxes shown in (**a**) and (**b**) are the regions chosen for this study: central India (15–25° N; 73–83° E), the Bay of Bengal (10–20° N; 85–95° E), and Southeast Asia (0–25° N; 100–125° E). (**f**) shows the decomposition of Q_{div} into radiative, latent, and sensible heat fluxes for the two regions.

in $P - E$. The shift of the LLJ can be seen more clearly in Fig. 9c, where the difference in winds between P_{min} and P_{max} is shown. Along the Equator, there exists an anomalous low-level easterly over the Indian Ocean. This meets an anomalous westerly from over equatorial Africa, at around 40° E. This indicates low-level convergence. Furthermore, on the same meridian, there exists a cyclonic circulation to the north (over the Middle East) and an anti-cyclonic circulation to the south (over Madagascar). This resembles the response of the winds to the heating of an atmospheric column as shown by Gill (1980).

Gill (1980) proposed a simple shallow water model on an equatorial β plane to elucidate the role of latent heating on surface winds. In order to represent convective heating due to latent heat release, he introduced mass divergence in the atmospheric column. When this model was forced with
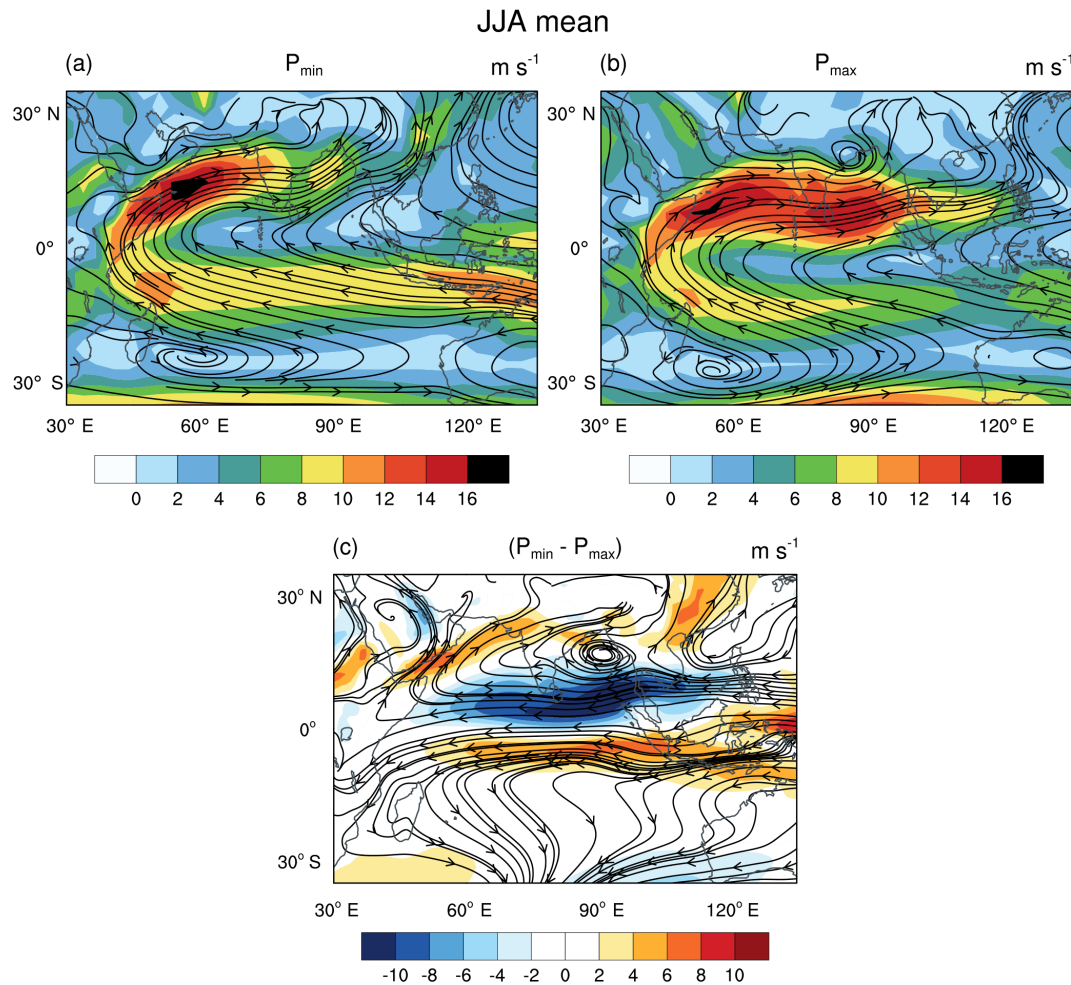
Figure 9. The JJA mean wind speed (850 hPa) in shading for **(a)** P_{min} and **(b)** P_{max}, with streamlines of the wind vector field superimposed. The difference of the winds between P_{min} and P_{max} is shown in **(c)**; 40° E longitude has a convergence at the Equator and cyclonic circulation over the Middle East. An anti-cyclonic circulation exists in the Southern Hemisphere over Madagascar. This is similar to the response of the atmosphere to equatorial plus off-equatorial heating (Gill, 1980).

"heating" over a region at the Equator and another region to the north of the Equator, it produced a Kelvin wave and a mixed Rossby-gravity wave. The Kelvin wave leads to an anomalous low-level easterly and an anomalous low-level westerly along the Equator. The easterly is to the east of the heat source and the westerly to the west of the heat source. These anomalous winds thus lead to low-level convergence at the Equator, near the region of the heat source. The mixed Rossby-gravity wave has a cyclonic circulation to the north of the Equator and an anti-cyclonic circulation to the south of the Equator. The wind response of EC-Earth hence, suggests that the wind patterns over the Indian subcontinent, are driven by atmospheric heating near the Equator and off-Equator. Examining Fig. 5a shows that the heat sources correspond to convective heating of the column due to increased precipitation over the West Equatorial Indian Ocean (WEIO) and over the Middle East (particularly the Red Sea). There

are, however, some important differences between EC-Earth and the Gill model. EC-Earth is a full GCM with non-zero mean background winds, whereas Gill model is linearized with respect to zero mean background winds. Thus, the EC-Earth's response includes non-linear terms as well.

To summarize, the decrease in Q_{div} over the Bay of Bengal is due to lower wind speeds. The winds decrease because of convective heating over west equatorial Indian Ocean and the Red Sea. The convection over the Red Sea is an extension of the African monsoon. Hence, we examine the factors which lead to an increase in precipitation over these regions. The prevailing conditions in the pre-monsoon month of May, leads to enhanced convection over these regions, later in the summer. Figure 10a and b, show the difference in Q_{div} and $P - E$ for the month of May. Figure 10b shows changes in $P - E$ in shading and the streamlines represent the changes in the wind direction. Q_{div} is higher over Africa, and this causes
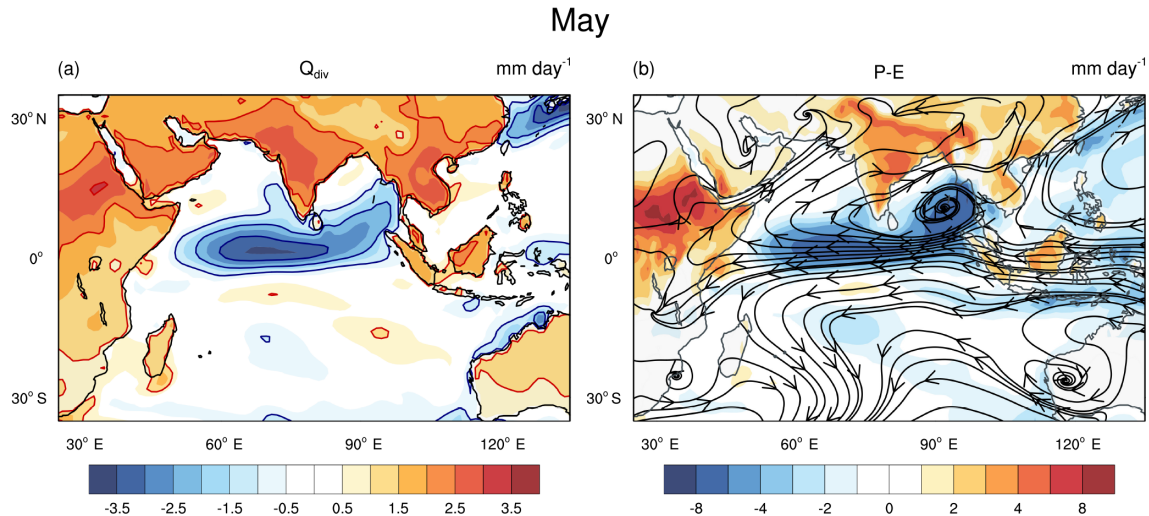
Figure 10. The difference between $P_{\min}$ and $P_{\max}$ in **(a)**, Q_{div} and **(b)**, $P - E$ along with streamlines of change in the wind, for the month of May. Note that the large increase in Q_{div} over Africa leads to an early onset of African monsoon. Thus, influencing the winds over the equatorial Indian Ocean.

early onset of the African monsoon (Fig. 10b) and changes the low-level winds along the eastern coast of Africa. The SST along the eastern coast depends on the coastal upwelling. The changes in winds thus reduce upwelling and increase SST. This enhances convection over the West Equatorial Indian Ocean, further leading to low-level convergence. This positive feedback is responsible for the convective heating that persists through the summer months. As the season advances from May onwards, the African monsoon propagates northward. The region of convection over the eastern side of Africa moves over to the Red Sea. This becomes the off-equatorial heat source.

3.3 Factors determining the response of Southeast Asian monsoon to precession

Shi et al. (2012) showed that the Southeast Asian monsoon and the Northeast Asian monsoon are out of phase owing to the El Niño-like SST pattern in $P_{\min}$. Here we are addressing the differences in the precipitation changes over Southeast Asia (land) and the adjacent ocean. The domain for Southeast Asia is shown in Fig. 8b. Based on the analysis using Eq. (15), we find that the increase (decrease) in $P - E$ over the land (ocean) grids is mainly due to the increase (decrease) in Q_{div} (Fig. 6). Even though Q_{div} is dominant, the contribution of TGMS is higher over Southeast Asia (oceanic regions) when compared to the Bay of Bengal. Once again decomposing Q_{div} into its component fluxes suggests a similar mechanism that leads to the Indian Bay of Bengal redistribution of precipitation (Fig. 8f). The increase in insolation leads to an increase in Q_{div} over the Southeast Asian land, whereas a decrease in LHF over the oceanic regions leads to a decrease in Q_{div}. The convective heating over WEIO and

the Red Sea leads to reduced winds, and hence decreased LHF in the northwestern Pacific.

4 Discussion

In this section, we have discussed the similarities between the sets of idealized experiments ($P_{\min}$, $P_{\max}$) vs. (Mid-Holocene (MH), Pre-Industrial (PI)). The MH and PI experiments were conducted with the same model EC-Earth, the details of which are available in Bosmans et al. (2012). The difference in solar forcing between MH and PI is similar to that between $P_{\min}$ and $P_{\max}$, albeit with a smaller amplitude (Fig. S2). Moreover, MH has an obliquity 0.66° higher than PI, and hence it contributes little to the total forcing (Fig. S2b). Previous research with models has shown that the climate response to precession is independent of obliquity (Tuenter et al., 2003). The climate of MH is therefore mainly driven by precession. The peak in the insolation difference between MH and PI is delayed by a month with respect to the insolation difference between $P_{\min}$ and $P_{\max}$. Hence the largest precipitation changes in MH occur about a month later than in $P_{\min}$ (Figs. 4 and S3). Therefore, we consider Jul–Aug–Sep averages for MH. The land-ocean shift in precipitation in MH is qualitatively explained by changes in Q_{div} (Fig. S4). Particularly, the displacement of precipitation from the Bay of Bengal to India is due to the same mechanism that drives these changes in $P_{\min}$ (Figs. S5, S6, and S7). The SE Asian monsoon also exhibits a land-ocean shift in rainfall. This is due to radiative heating over land as well as the ocean. This suggests that the cloud radiative feedbacks are stronger for the SE Asian monsoon. The changes in LHF are, however, due to the same reason as in $P_{\min}$. We also performed the analysis for a set of obliquity experiments $T_{\max}$

and $T_{\min}$, corresponding to the maximum and minimum tilt, with eccentricity set to zero (Bosmans et al., 2015). The tropical precipitation shows a land-ocean shift in precipitation, but the amplitude of change is small compared to the precession experiments (Fig. S9). The mechanisms leading to this shift are different for obliquity and precession (Figs. S10 and S11).

Models with different levels of complexities: QTCM (Hsu et al., 2010), Quasi-geostrophic model EC-Bilt (Tuenter et al., 2003), GCM with slab ocean (Battisti et al., 2014) and finally the fully coupled model EC-Earth (Bosmans et al., 2018) have all shown a shift in precipitation between land and ocean, when subjected to the precessional forcing. However, there are no proxies for precipitation over oceans to verify this. Since the climate over islands is influenced by the surrounding oceans, proxies obtained from islands can be thought of as a representation of climate over the surrounding ocean. A speleothem chronology from the Baratang cave in the Andaman Islands (Laskar et al., 2013) in this regard, represents precipitation over the Bay of Bengal. This chronology goes back to 4000 years before present and shows a long-term decreasing trend in precipitation as we move back in time. The time period corresponding to 4 ka being closer to MH has higher summer insolation and proxies over Indian continent register an increase in precipitation (Ramesh, 2001; Patnaik et al., 2012; Zhang et al., 2016; Kathayat et al., 2017). This suggests that the GCMs and observations indicate the response of Indian land mass is different from the response in the Bay of Bengal.

5 Summary and conclusions

Using a simple model for ITCZ, we have interpreted the response of a high resolution fully coupled model EC-Earth to precession. The changes in precipitation can be attributed to either the changes in total energy fluxes going into the column (Q_{div}) or the changes in vertical stability of the atmosphere (TGMS). We have included the horizontal advection terms in the calculation of TGMS, which were originally assumed to be small (Neelin and Held, 1987). This allows us to use the simple ITCZ model for relatively smaller domains, where horizontal advection terms can be large. TGMS represents the total transport of the MSE. In places where the horizontal transport is weak, TGMS is the same as GMS. Changes in precession provide an initial forcing. The final response of the precipitation is due to this initial forcing and the consequent feedbacks. These feedbacks are in the form of changes in surface energy fluxes and changes in stability of the atmosphere. In agreement with Chamales (2014), we find that precipitation changes between precession extremes over the whole tropics are, due to changes in Q_{div} over land and due to TGMS over the ocean. This generalization is, however, not valid for smaller regions. Within the domain of the South Asian monsoon, insolation drives changes

in Q_{div} over the land, whereas latent heat fluxes contribute most over the oceans. Particularly, the decrease in LHF over the Bay of Bengal and the northwestern Pacific is associated with the weakening of the low-level westerlies over these regions. These changes in westerlies are driven by convective heating of the atmospheric column over the western equatorial Indian Ocean and the Middle East. There are, however, regions where the changes in TGMS is the main cause of the changes in precipitation (e.g., Africa and the Arabian Sea). We have demonstrated that the simple ITCZ model can be used to explain the precipitation response for any orbital configuration (e.g., MH, maximum and minimum obliquity experiments).

References

Balsamo, G., Beljaars, A., Scipal, K., Viterbo, P., van den Hurk, B., Hirschi, M., and Betts, A. K.: A revised hydrology for the ECMWF model: Verification from field site to terrestrial water storage and impact in the Integrated Forecast System, J. Hydrometeorol., 10, 623–643, 2009.

Battisti, D., Ding, Q., and Roe, G.: Coherent pan-Asian climatic and isotopic response to orbital forcing of tropical insolation, J. Geophys. Res.-Atmos., 119, 11997–12020, 2014.

Bechtold, P., Köhler, M., Jung, T., Doblas-Reyes, F., Leutbecher, M., Rodwell, M. J., Vitart, F., and Balsamo, G.: Advances in simulating atmospheric variability with the ECMWF model: From

synoptic to decadal time-scales, Q. J. Roy. Meteor. Soc., 134, 1337–1351, 2008.

Berger, A.: Long-term variations of daily insolation and Quaternary climatic changes, J. Atmos. Sci., 35, 2362–2367, 1978.

Boos, W. R. and Kuang, Z.: Mechanisms of poleward propagating, intraseasonal convective anomalies in cloud system–resolving models, J. Atmos. Sci., 67, 3673–3691, 2010.

Bordoni, S. and Schneider, T.: Monsoons as eddy-mediated regime transitions of the tropical overturning circulation, Nat. Geosci., 1, 515–519, 2008.

Bosmans, J. H. C., Drijfhout, S. S., Tuenter, E., Lourens, L. J., Hilgen, F. J., and Weber, S. L.: Monsoonal response to mid-holocene orbital forcing in a high resolution GCM, Clim. Past, 8, 723–740, https://doi.org/10.5194/cp-8-723-2012, 2012.

Bosmans, J., Drijfhout, S., Tuenter, E., Hilgen, F., and Lourens, L.: Response of the North African summer monsoon to precession and obliquity forcings in the EC-Earth GCM, Clim. Dynam., 44, 279–297, 2015.

Bosmans, J., Erb, M., Dolan, A., Drijfhout, S., Tuenter, E., Hilgen, F., Edge, D., Pope, J., and Lourens, L.: Response of the Asian summer monsoons to idealized precession and obliquity forcing in a set of GCMs, Quaternary Sci. Rev., 188, 121–135, 2018.

Braconnot, P., Marzin, C., Grégoire, L., Mosquet, E., and Marti, O.: Monsoon response to changes in Earth's orbital parameters: comparisons between simulations of the Eemian and of the Holocene, Clim. Past, 4, 281–294, https://doi.org/10.5194/cp-4-281-2008, 2008.

Caley, T., Roche, D. M., and Renssen, H.: Orbital Asian summer monsoon dynamics revealed using an isotope-enabled global climate model, Nat. Commun., 5, 5371, https://doi.org/10.1038/ncomms6371, 2014.

Chamales, K. A.: The effects of orbital precession on tropical precipitation, MS thesis, Dept. of Meteorology and Physical Oceanography, University of Miami, 63 pp., 2014.

Chou, C. and Neelin, J. D.: Mechanisms of global warming impacts on regional tropical precipitation, J. Climate, 17, 2688–2701, 2004.

Chou, C., Neelin, J. D., Lohmann, U., and Feichter, J.: Local and remote impacts of aerosol climate forcing on tropical precipitation, J. Climate, 18, 4621–4636, 2005.

Chou, C., Neelin, J. D., Tu, J.-Y., and Chen, C.-T.: Regional tropical precipitation change mechanisms in ECHAM4/OPYC3 under global warming, J. Climate, 19, 4207–4223, 2006.

Clement, A. C., Hall, A., and Broccoli, A.: The importance of precessional signals in the tropical climate, Clim. Dynam., 22, 327–341, 2004.

Cruz Jr., F. W., Burns, S. J., Karmann, I., Sharp, W. D., Vuille, M., Cardoso, A. O., Ferrari, J. A., Dias, P. L. S., and Viana Jr., O.: Insolation-driven changes in atmospheric circulation over the past 116,000 years in subtropical Brazil, Nature, 434, 63–66, 2005.

Donohoe, A., Marshall, J., Ferreira, D., and Mcgee, D.: The relationship between ITCZ location and cross-equatorial atmospheric heat transport: From the seasonal cycle to the Last Glacial Maximum, J. Climate, 26, 3597–3618, 2013.

Gadgil, S.: The monsoon system: Land–sea breeze or the ITCZ?, J. Earth Syst. Sci., 127, 1–29, https://doi.org/10.1007/s12040-017-0916-x, 2018.

Gill, A.: Some simple solutions for heat-induced tropical circulation, Q. J. Roy. Meteor. Soc., 106, 447–462, 1980.

Hazeleger, W., Severijns, C., Semmler, T., Ştefănescu, S., Yang, S., Wang, X., Wyser, K., Dutra, E., Baldasano, J. M., Bintanja, R., Bougeault, P., Caballero, R., Ekman, A. M. L., Christensen, J. H., van den Hurk, B., Jimenez, P., Jones, C., Kållberg, P., Koenigk, T., McGrath, R., Miranda, P., van Noije, T., Palmer, T., Parodi, J. A., Schmith, T., Selten, F., Storelvmo, T., Sterl, A., Tapamo, H., Vancoppenolle, M., Viterbo, P., and Willén, U.: EC-Earth: a seamless earth-system prediction approach in action, B. Am. Meteorol. Soc., 91, 1357–1363, 2010.

Hazeleger, W., Wang, X., Severijns, C., Ştefănescu, S., Bintanja, R., Sterl, A., Wyser, K., Semmler, T., Yang, S., van den Hurk, B., van Noije, T., van der Linden, E., and van der Wiel, K.: EC-Earth V2. 2: description and validation of a new seamless earth system prediction model, Clim. Dynam., 39, 2611–2629, 2012.

Hsu, Y.-H., Chou, C., and Wei, K.-Y.: Land–ocean asymmetry of tropical precipitation changes in the mid-Holocene, J. Climate, 23, 4133–4151, 2010.

Kang, S. M., Held, I. M., Frierson, D. M. W., and Zhao, M.: The response of the ITCZ to extratropical thermal forcing: Idealized slab-ocean experiments with a GCM, J. Climate, 21, 3521–3532, 2008.

Kathayat, G., Cheng, H., Sinha, A., Yi, L., Li, X., Zhang, H., Li, H., Ning, Y., and Edwards, R. L.: The Indian monsoon variability and civilization changes in the Indian subcontinent, Science Advances, 3, e1701296, https://doi.org/10.1126/sciadv.1701296, 2017.

Kutzbach, J., Liu, X., Liu, Z., and Chen, G.: Simulation of the evolutionary response of global summer monsoons to orbital forcing over the past 280,000 years, Clim. Dynam., 30, 567–579, 2008.

Kutzbach, J. E.: Monsoon climate of the early Holocene: climate experiment with the earth's orbital parameters for 9000 years ago, Science, 214, 59–61, 1981.

Laskar, A. H., Yadava, M., Ramesh, R., Polyak, V., and Asmerom, Y.: A 4 kyr stalagmite oxygen isotopic record of the past Indian Summer Monsoon in the Andaman Islands, Geochem. Geophy. Geosy., 14, 3555–3566, 2013.

Madec, G.: NEMO, the ocean engine, Note du Pole de modelisation, Institut Pierre-Simon Laplace (IPSL), France, No. 27 ISSN No. 1288–1619, 2008.

Merlis, T. M., Schneider, T., Bordoni, S., and Eisenman, I.: Hadley circulation response to orbital precession. Part II: Subtropical continent, J. Climate, 26, 754–771, 2013.

Mohtadi, M., Prange, M., and Steinke, S.: Palaeoclimatic insights into forcing and response of monsoon rainfall, Nature, 533, 191–199, 2016.

Neelin, J. D. and Held, I. M.: Modeling tropical convergence based on the moist static energy budget, Mon. Weather Rev., 115, 3–12, 1987.

Patnaik, R., Gupta, A. K., Naidu, P. D., Yadav, R., Bhattacharyya, A., and Kumar, M.: Indian monsoon variability at different time scales: marine and terrestrial proxy records, Proceedings of the Indian National Science Academy, 78, 535–547, 2012.

Pokras, E. M. and Mix, A. C.: Earth's precession cycle and Quaternary climatic change in tropical Africa, Nature, 326, 486–487, 1987.

Privé, N. C. and Plumb, R. A.: Monsoon dynamics with interactive forcing. Part I: Axisymmetric studies, J. Atmos. Sci., 64, 1417–1430, 2007a.

Privé, N. C. and Plumb, R. A.: Monsoon dynamics with interactive forcing. Part II: Impact of eddies and asymmetric geometries, J. Atmos. Sci., 64, 1431–1442, 2007b.

Ramesh, R.: High resolution Holocene monsoon records from different proxies: An assessment of their consistency, Curr. Sci. India, 81, 1432–1436, 2001.

Schneider, T., Bischoff, T., and Haug, G. H.: Migrations and dynamics of the intertropical convergence zone, Nature, 513, 45–53, 2014.

Shi, Z.: Response of Asian summer monsoon duration to orbital forcing under glacial and interglacial conditions: Implication for precipitation variability in geological records, Quaternary Sci. Rev., 139, 30–42, 2016.

Shi, Z., Liu, X., and Cheng, X.: Anti-phased response of northern and southern East Asian summer precipitation to ENSO modulation of orbital forcing, Quaternary Sci. Rev., 40, 30–38, 2012.

Sterl, A., Bintanja, R., Brodeau, L., Gleeson, E., Koenigk, T., Schmith, T., Semmler, T., Severijns, C., Wyser, K., and Yang, S.: A look at the ocean in the EC-Earth climate model, Clim. Dynam., 39, 2631–2657, 2012.

Sun, Y., Zhou, T., Ramstein, G., Contoux, C., and Zhang, Z.: Drivers and mechanisms for enhanced summer monsoon precipitation over East Asia during the mid-Pliocene in the IPSL-CM5A, Clim. Dynam., 46, 1437–1457, 2016.

Sun, Y., Ramstein, G., Li, L. Z., Contoux, C., Tan, N., and Zhou, T.: Quantifying East Asian summer monsoon dynamics in the ECP4. 5 scenario with reference to the mid-Piacenzian warm period, Geophys. Res. Lett., 45, 12–523, 2018.

Tuenter, E., Weber, S., Hilgen, F., and Lourens, L.: The response of the African summer monsoon to remote and local forcing due to precession and obliquity, Global Planet. Change, 36, 219–235, 2003.

Tuenter, E., Weber, S., Hilgen, F., Lourens, L., and Ganopolski, A.: Simulation of climate phase lags in response to precession and obliquity forcing and the role of vegetation, Clim. Dynam., 24, 279–295, 2005.

Valcke, S. and Morel, T.: OASIS and PALM, the CERFACS couplers, Tech. rep., CERFACS, 2006.

Wang, X., Auler, A. S., Edwards, R., Cheng, H., Ito, E., Wang, Y., Kong, X., and Solheid, M.: Millennial-scale precipitation changes in southern Brazil over the past 90,000 years, Geophys. Res. Lett., 34, L23701, https://doi.org/10.1029/2007GL031149, 2007.

Wang, Y., Cheng, H., Edwards, R. L., Kong, X., Shao, X., Chen, S., Wu, J., Jiang, X., Wang, X., and An, Z.: Millennial-and orbital-scale changes in the East Asian monsoon over the past 224,000 years, Nature, 451, 1090–1093, 2008.

Weber, S. and Tuenter, E.: The impact of varying ice sheets and greenhouse gases on the intensity and timing of boreal summer monsoons, Quaternary Sci. Rev., 30, 469–479, 2011.

Zhang, E., Wang, Y., Sun, W., and Shen, J.: Holocene Asian monsoon evolution revealed by a pollen record from an alpine lake on the southeastern margin of the Qinghai-Tibetan Plateau, China, Clim. Past, 12, 415–427, https://doi.org/10.5194/cp-12-415-2016, 2016.

Zhao, Y. and Harrison, S.: Mid-Holocene monsoons: a multi-model analysis of the inter-hemispheric differences in the responses to orbital forcing and ocean feedbacks, Clim. Dynam., 39, 1457–1487, 2012.